Geophysical Research Letters®

Key Points:
- Decoupled clouds can notably delay the process of eroding nocturnal inversion by suppressing surface fluxes
- Cloud-top radiative cooling caused by coupled clouds facilitates the formation of the unstable boundary layer in the earlier morning
- Cloud-surface coupling notably affects the diurnal variation of the boundary layer by altering the phase transition of the boundary layer

Author Contributions:
Conceptualization: Tianning Su, Zhanqing Li, Youtong Zheng
Investigation: Tianning Su
Methodology: Tianning Su
Supervision: Zhanqing Li
Validation: Tianning Su
Visualization: Tianning Su
Writing – original draft: Zhanqing Li, Youtong Zheng
Writing – review & editing: Tianning Su, Zhanqing Li, Youtong Zheng

Cloud-Surface Coupling Alters the Morning Transition From Stable to Unstable Boundary Layer

Tianning Su[1] , **Zhanqing Li[1]** , and **Youtong Zheng[2,3]**

[1]Department of Atmospheric and Oceanic Sciences, University of Maryland, College Park, College Park, MD, USA, [2]Department of Atmospheric and Earth Science, University of Houston, Houston, TX, USA, [3]Program in Atmospheric and Oceanic Sciences, Princeton University, Princeton, NJ, USA

Abstract Due to surface heating, the morning boundary layer transits from stable to neutral or convective conditions, exerting critical influences on low tropospheric thermodynamics. Low clouds closely interact with the boundary layer development, yet their interactions bear considerable uncertainties. Our study reveals that cloud-surface coupling alters the morning transition from stable to unstable boundary layer and thus notably affects the diurnal variation of the boundary layer. Specifically, due to the reduction in surface fluxes, decoupled clouds can delay the process of eroding nocturnal inversion by 0.8-hr and even prevent the transition of the boundary layer from happening for 12% of decoupled cases, keeping the boundary layer in a stable state during the noontime. On the other hand, when clouds are coupled with the surface, cloud-top radiative cooling can directly cool the upper boundary layer to facilitate sub-cloud convection, leading to an unstable boundary layer in the earlier morning.

Plain Language Summary Low clouds closely interact with the planetary boundary layer, yet their interactions bear considerable uncertainties. Our study reveals that cloud-surface coupling plays an important role in regulating the diurnal variation of boundary layer. In particular, cloud-surface coupling affects the energy budget of the land-atmosphere system and further alters the transition from the stable boundary layer to the unstable boundary layer during the morning. Due to the reduction in surface fluxes, decoupled clouds can notably delay the process of eroding nocturnal inversion, keeping the boundary layer in a relatively stable state. On the other hand, when clouds are coupled with the surface, cloud-top radiative cooling can directly cool the upper boundary layer to facilitate convection, leading to an unstable boundary layer in the earlier morning.

1. Introduction

In the morning, the planetary boundary layer (PBL) usually experiences a transition from stable to neutral or unstable conditions that exert important influences on the convection process and low tropospheric thermodynamics (Garratt, 1994; Guo et al., 2021; Wallace & Hobbs, 2006; Wyngaard & Coté, 1974). The PBL transition results from eroding the nocturnal temperature inversion due to surface heating. Following Stull (1988), we refer to the full transition from stable to unstable PBL as the "phase transition." Before the phase transition, PBLH increases slowly because of the strong nocturnal temperature inversion near the surface, with the depth ranging from tens of meters to a few hundred meters. After the phase transition, PBL quickly rises and reaches the top of the residual layer rapidly because of the small potential temperature gradient in the residual layer (Chu et al., 2019; Garrett, 1982; Su, Li, et al., 2022).

Although such a conceptual evolution of the PBL transition has been well established, the real-world PBL behaves more complexly. While the morning PBL is typically stable, it can also be well mixed by various factors, one of which is the cloud. Cloud can significantly affect the radiation budget and thus modulate the surface fluxes. Meanwhile, cloud-top radiative cooling (CTRC) is another crucial factor driving turbulence within the boundary layer (Deardorff, 1976; Hogan et al., 2009; Nicholls, 1989). The cloud-shading effect and CTRC jointly dictate PBL development.

Despite previous investigations of the interactions between clouds and PBL development (Bacmeister et al., 2006; Garrett, 1982; Zheng et al., 2021), the response to the phase transition of morning PBL to clouds has not been well understood. By using the comprehensive field observations, we can analyze the impacts of clouds on radiation budget and surface fluxes. Furthermore, based on the observations and theoretical calculations, we aim to illuminate the role of cloud-surface coupling in the phase transition of the morning PBL. These analyses are

important for the research community for the following reasons: (a) The transition of PBL is a critical aspect of the diurnal cycle of the PBL, influencing the exchange of heat, moisture, and momentum between the surface and the atmosphere. (b) The PBL transition is also closely linked to cloud development, as the thermodynamic stability of the PBL can affect the initiation and entrainment of convection. Therefore, understanding how clouds alter the PBL transition is crucial for improving our understanding of boundary layer processes, cloud development and the interaction between land and atmosphere.

2. Data and Methods

2.1. Observations at the SGP Site

The U.S. Department of Energy's Atmospheric Radiation Measurement (ARM) has been made in the Southern Great Plains (SGP) of Oklahoma (36.607°N, 97.488°W) since the late 1980s. Being the most extensive and well-equipped climate research facility in the world, it has provided ample, highly accurate observations for atmospheric and climate studies. The study used comprehensive measurements of PBL, clouds, radiation, and meteorological variables from 1999 to 2019 at the SGP site. These datasets include: (a) the profiles of potential temperature, (b) Active Remote Sensing of Clouds, (c) cloud Optical Properties from the Multifilter Shadowband Radiometer, (d) radiation budget and surface fluxes, (e) soil moisture, (f) sixty-meter meteorological tower. The detailed descriptions of these archived data sets (https://adc.arm.gov/discovery) can be found in Supporting Information S1.

2.2. PBL Depth and Cloud-Surface Coupling From Lidar

We have developed remote sensing methods to estimate the PBLH and cloud-surface coupling over land (Su, Zheng, & Li, 2022; Su et al., 2020), whose principles of determination are briefly introduced here. The method simultaneously retrieves coupled states and PBLH variability from the micropulse lidar by taking account of both the temporal continuity and vertical backscatter signals of the PBL. By considering the temporal variations of PBL, the PBL top is identified as a step signal in the function of signal gradient and wavelet covariance transform obtained from lidar backscatters (Brooks, 2003).

Furthermore, we used the lidar-derived PBLH, the cloud position, and the lifted condensation level (LCL) to identify coupled or decoupled clouds (Su, Zheng, & Li, 2022). For a coupled cloud, the turbulent fluxes generated from surface can reach the cloud-base and affect the cloud development, leading to a turbulent coupling between surface fluxes, PBL, and cloud. Otherwise, the cloud is in the decoupled state. Cloud is considered as the coupled cloud if cloud-base height (CBH) is consistent with the previous PBL top and LCL, where LCL is computed from meteorological parameters (temperature, RH, pressure) at the surface level (Romps, 2017). We also assimilate the 06:30 local time (LT) radiosonde, which provides the standard identification of cloud-surface coupling during the morning. Based on the radiosonde data, we can use the potential temperature profiles to identify cloud-surface coupling. If there is a potential temperature inversion between the cloud base and the PBL top, the cloud is considered to be in a decoupled state, or it is coupled with the surface. For coupled cases, we use the cloud position to infer PBLH under cloudy conditions. The cloud top is considered as the PBLH for stratiform clouds, while CBH is used to calculate PBLH for active cumulus clouds. As a diagnosis parameter, the cloud-surface coupling retrieved from lidar demonstrates good consistency with those derived from radiosonde with about 10% differences (Su, Zheng, & Li, 2022).

To investigate the impacts of clouds on PBL phase transitions, we select the cases when clouds occur before the transitions. Meanwhile, we only analyze the cases when clouds maintain more than 50% of the time from 07:00–11:00 LT. Driven by the PBL convection, coupled cumulus only occurs under unstable conditions and is not directly related to the PBL transition from stable to unstable conditions. Thus, we primarily focused on the coupled stratiform clouds. As precipitation would disturb the lidar measurements, we also exclude the rainy cases. For analyzing the cloud radiative effects, we also require continuous measurements of cloud, radiation, radiosonde, and soil measurements during the daytime. Among the data under study, 425 and 322 days had decoupled and coupled clouds meeting the requirements of our study, respectively.

2.3. Cloud Radiative Forcing From a Radiative Transfer Model

In this study, we use the Santa Barbara discrete ordinates radiative transfer Atmospheric Radiative Transfer (SBDART) model (Ricchiazzi et al., 1998) to estimate the cloud radiative forcing (CRF). The vertical profiles
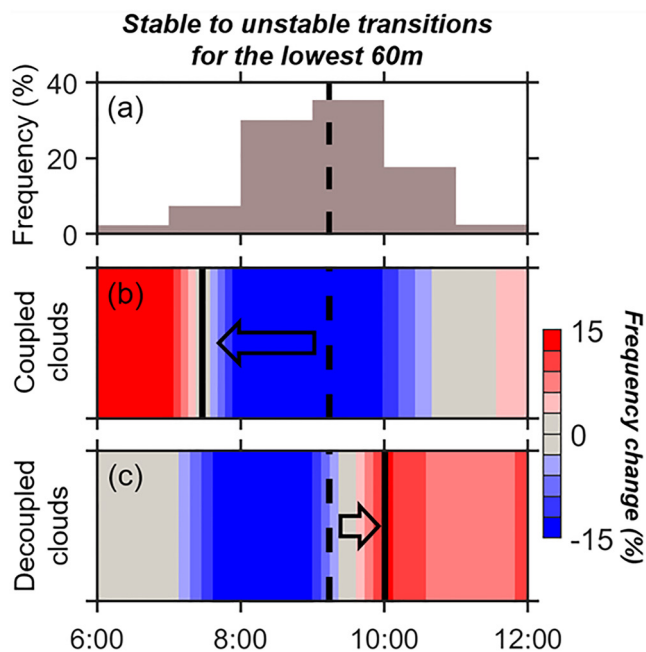
Figure 1. (a) The frequencies of occurrence in phase transitions for the lowest 60 m near the surface under clear-sky conditions; (b) changes in the frequencies of occurrence in phase transitions between the clear-sky and coupled cloudy conditions; (c) same as (b) but for decoupled cloud conditions. Solid dash lines mark the median values of the phase transition.

of humidity, pressure, and temperature are obtained from the closest radiosonde. The CRF represents the differences in the radiative fluxes between cloudy and clear conditions. The net CRF at surface is calculated as the sum of longwave CRF and shortwave CRF, including direct and diffuse components. We calculate the CTRC as the divergence of net radiative flux across the cloud top (Zheng et al., 2018).

2.4. Estimating Surface Fluxes From a Deep-Learning-Based Surface Model

Land surface models are conventionally used to simulate land surface processes. However, the land surface model is associated with complex interactions between the surface and meteorology, leading to uncertainties from multiple sources (Bonan, 1996; Dumedah & Walker, 2014; Prihodko et al., 2008). As emerging powerful tools, deep learning or machine learning has been used to estimate the surface fluxes (Alemohammad et al., 2017; Jung et al., 2011).

This study adopted a deep neural network (DNN) to retrieve sensible heat from multiple inputs, including surface radiation budget, soil moisture, atmospheric humidity, seasonality, and time. Due to the nonlinear relationship among various inputs, we use the Bayesian regularization approach in the deep learning model to track the complex relationship between the surface parameter and meteorological conditions (Burden & Winkler, 2008). The structure and input/output parameters of the DNN model are presented in Figure S1 in Supporting Information S1. We used 70% of the total samples for training the DNN model, then utilized the remaining 30% of the data set for evaluation. The cross-validation of the DNN model (Rodriguez et al., 2009) is presented in Figure S2 in Supporting Information S1 with a correlation coefficient of ∼0.9.

In this way, the linkage between surface solar radiation and surface fluxes is established over the SGP site. We use the SBDART model to estimate the impacts of clouds on the net surface radiation budget (Section 2.3). Furthermore, by changing the net surface radiation in the DNN model, we can calculate the surface sensible heat with or without cloud radiative effects. Thus, we can estimate the impacts of clouds on the energy supplied from sensible heat.

3. Results

3.1. Stable to Unstable Transition in the Lowest 60-m

By utilizing the 60-m tower over the SGP site, the evolution of thermodynamics in the PBL layer is investigated throughout the phase transition. We use the potential temperature differences ($\Delta\theta = \theta_{surf} - \theta_{60m}$) between surface and 60m to diagnose the layer stability and identify the stable layer when $\Delta\theta$ is less than 0.1 K. The stable to unstable transitions occur when $\Delta\theta$ increases to exceed 0.1 K during the daytime. Note that the threshold of 0.1 K has been used by Zhang et al. (2018) to identify the state of the PBL (i.e., stable PBL, neutral PBL, and convective PBL). We adopted this threshold to investigate the transition from stable to unstable PBLs. The frequency of stable to unstable transitions of the lowest 60 m presents in Figure 1a. The peak of this transition occurs around 09:10 LT for all the cases examined. The transition differs between clear and cloudy conditions, as well as between coupled and decoupled conditions. The differences in the frequencies of transition occurrence between cloudy and clear skies are presented in Figures 1b and 1c for coupled and decoupled conditions, respectively. Under the coupled conditions, it appeared much earlier than under clear-sky conditions, and the opposite is the case for decoupled clouds. Under coupled conditions, the transition from stable to unstable conditions occurs in the early morning (06:00-08:00 LT) or during the previous night. Under the decoupled conditions, the transition is delayed by about 0.8 hr. Such notable disparity indicates that cloud-surface coupling may have a critical impact
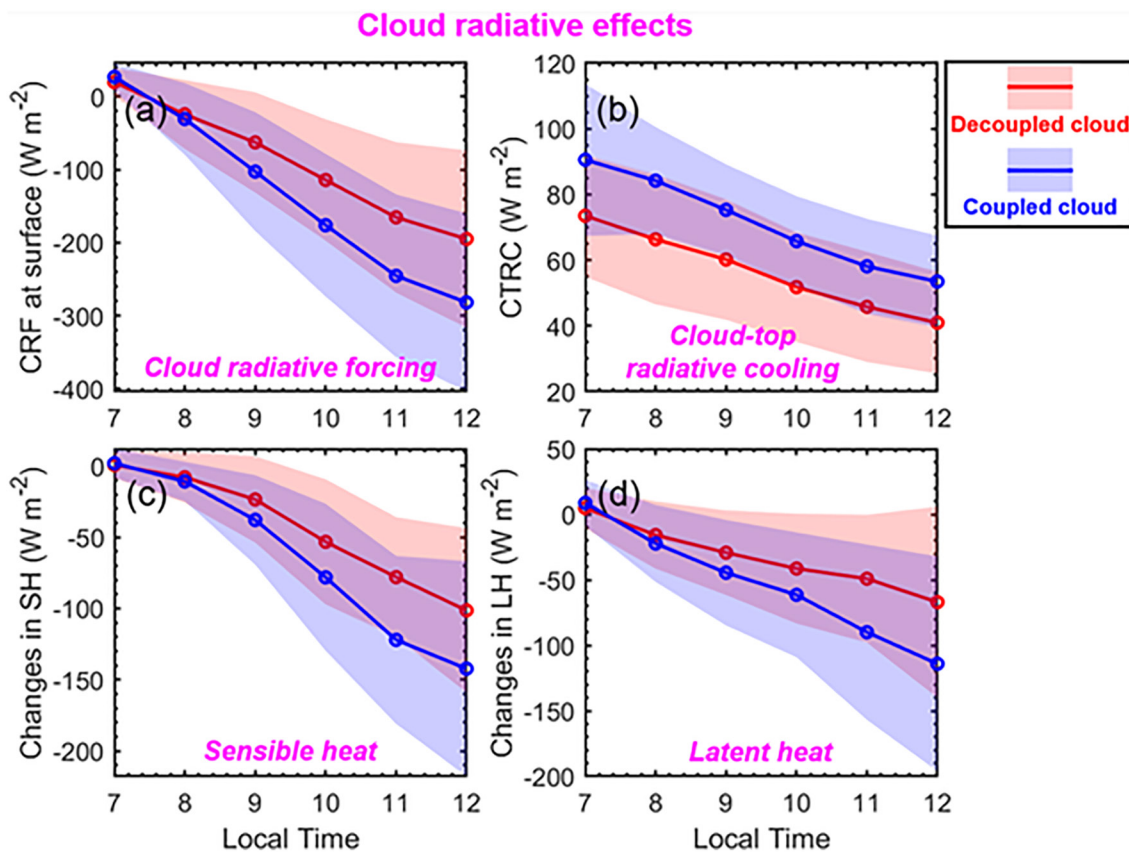
Figure 2. (a) Variations of the cloud radiative forcing (CRF) at the surface level for coupled and decoupled clouds during 07:00-12:00 local time (LT). (b) Same as (a), but for cloud-top radiative cooling (CTRC). (c) Same as (a), but for cloud-induced changes in surface sensible heat (SH). (d) Same as (a), but for cloud-induced changes in surface latent heat (LH).

on modulating the phase transition processes of PBL that are closely associated with the cloud radiative effects and PBL thermodynamics.

3.2. Analyses of Cloud Radiative Forcing

To investigate the impacts of the cloud on PBL phase transition, we analyzed cloud-induced changes in net CRF at surface (Figure 2a) and cloud-top (Figure 2b), surface sensible (Figure 2c), and latent heat (Figure 2d) under the coupled and decoupled conditions. The different effects of diffuse and direct radiations at shortwave and longwave are presented in Figure S3 in Supporting Information S1. As the net effect, CRF is significant both at the surface and at the cloud top, especially under coupled conditions. The former can cool the surface, whereas the latter is referred to as CTRC caused by enhanced thermal radiation emission. In addition, the reduction in surface shortwave radiation lowers both sensible and latent heat, which is especially significant for coupled clouds that dramatically diminish sensible heat (Figure 2c and Figure S4 in Supporting Information S1).

The linkage between the CRF and PBL thermodynamics can be seen from the heating rates measured by changes in potential temperatures under coupled and decoupled conditions (Figure 3). During the nighttime, the cooling effect is notable in the PBL top caused by CTRC (Figure 3a), while horizontal transport has a small contribution to the cooling effect (Figure S5 in Supporting Information S1). Such a cooling effect at the PBL top increases the temperature gradient in the sub-cloud layer, thus enhancing the convection in the sub-cloud layer and further facilitating cloud development during the nighttime, even in the absence of surface heating. As CTRC is hampered by the increased solar insolation (Zheng et al., 2018), the magnitude of CTRC is smaller during the daytime (Figures 2b and 3).
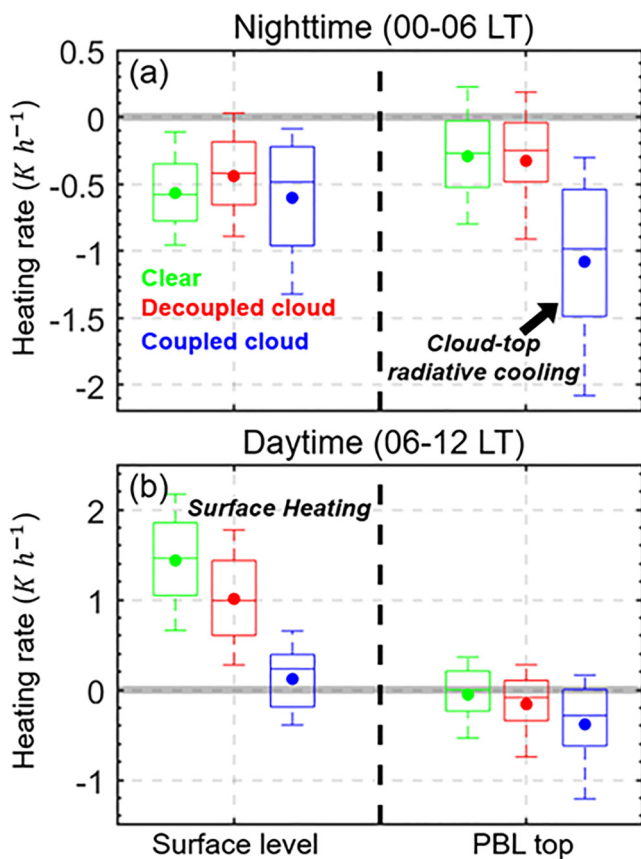
Figure 3. The box-and-whisker plots demonstrate the percentiles (10, 25, 50, 75, and 90 respectively) of heating rate at the surface and the PBL top under clear sky (green), decoupled cloud conditions (red), and coupled cloud conditions (blue) during (a) the nighttime (00:00-06:00 LT) and (b) the daytime (06:00-12:00 LT). The heating rate is calculated as the change rate in the potential temperature between the beginning and the end of two periods based on radiosonde. The notable effects of cloud-top radiative cooling during nighttime (a) and surface heating during daytime (b) are marked.

On the other hand, due to the decoupling between cloud and PBL, CTRC of decoupled clouds only exerts cooling effects on the free atmosphere and thus cannot directly affect PBL thermodynamics. The strong inversion in the sub-cloud layer serves as a barrier to limiting the exchange of heat fluxes between PBL and cloud. During the daytime, surface heating generally plays a dominant role in PBL development that is suppressed by clouds under both coupled and decoupled conditions (Figure 3b).

3.3. The Linkage Between Cloud-Surface Coupling and PBL Evolution

CTRC and surface heating jointly regulate the phase transition of PBL evolution under cloudy conditions, whose mechanisms are further exploited here in the context of cloud-surface coupling. Figures 4a and 4b present the cloud-induced heating rates under coupled and decoupled clouds. Cloud can exert strong cooling effects at the cloud top, along with a slight heating effect at the cloud base. When stratiform clouds are coupled with PBL, the notable cooling effect can trigger the vertical mixing within PBL along with the entrainment process. Furthermore, as CTRC cools the PBL top under coupled conditions, it can enhance the temperature inversion capping the cloud and PBL, leading to suppression in the PBL growth (Lock, 1998).

Under the decoupled conditions, the CTRC is decoupled with the PBL and cannot affect PBL development (Figure 4b). Under this scenario, the phase transition of PBL is controlled by surface heating. We may thus argue that transition from stable to unstable conditions in the PBL is driven primarily by the CTRC under coupled cloud conditions, and by surface heating under decoupled cloudy conditions and clear-sky conditions.

To understand the role of surface heating in modulating phase transitions under clear-sky and decoupled conditions, we analyze the energy balance and its key components. Following Stull (1988), we used the morning radiosonde to calculate the required energy for the phase transition, which equals the vertical integral of temperature profiles within the inversion layer (Figure S6 in Supporting Information S1). The time integral of surface sensible heat fluxes denotes the total energy supply from surface heating. This diagram requires surface heating as the dominant energy source for PBL development (Stull, 1988), and thus is only valid for the clear-sky and decoupled clouds. Figure 4c presents the supplied and required energy under the clear-sky and decoupled clouds derived from observations. To demonstrate cloud impacts, we calculated the supplied energy (black line in Figure 4c) from surface sensible heat after excluding the cloud radiative effects (see Section 2.4).

As the phase transition of PBL occurs when the supplied energy exceeds the required energy, the suppression of supplied energy notably delays the phase transition of PBL under the decoupled condition. To quantitatively demonstrate this, we present the probability density functions of the phase transition time for decoupled clouds, as well as those by excluding cloud impacts as mentioned above (Figure 4d). On average, decoupled clouds delay the phase transition by 51 min and lead to 12% of cases where the phase transition occurs after 12:00 LT, preventing a typical phase transition during the morning.

The changes in phase transitions induced by coupled clouds profoundly affect the PBL evolution. Figure 5 presents the statistical variation in PBL and $\Delta\theta$ in the lowest 60 m, representing the thermodynamic stability of the surface layer. Here, we also calculate the PBL growth rate before/after the phase transitions and separately consider the clear-sky conditions, the decoupled condition, and the coupled condition. For the clear-sky condition, the phase transition generally occurs around 09:40 LT (Figure 5a). After the phase transition, the PBL growth rate substantially increases, causing the PBL top rises to the top of the residual layer fueled by surface heating.

The PBL evolution under the decoupled condition is notably different compared to the clear sky condition (Figure 5b), for which PBL grows quickly after the phase transition. In contrast, the PBL under the decoupled
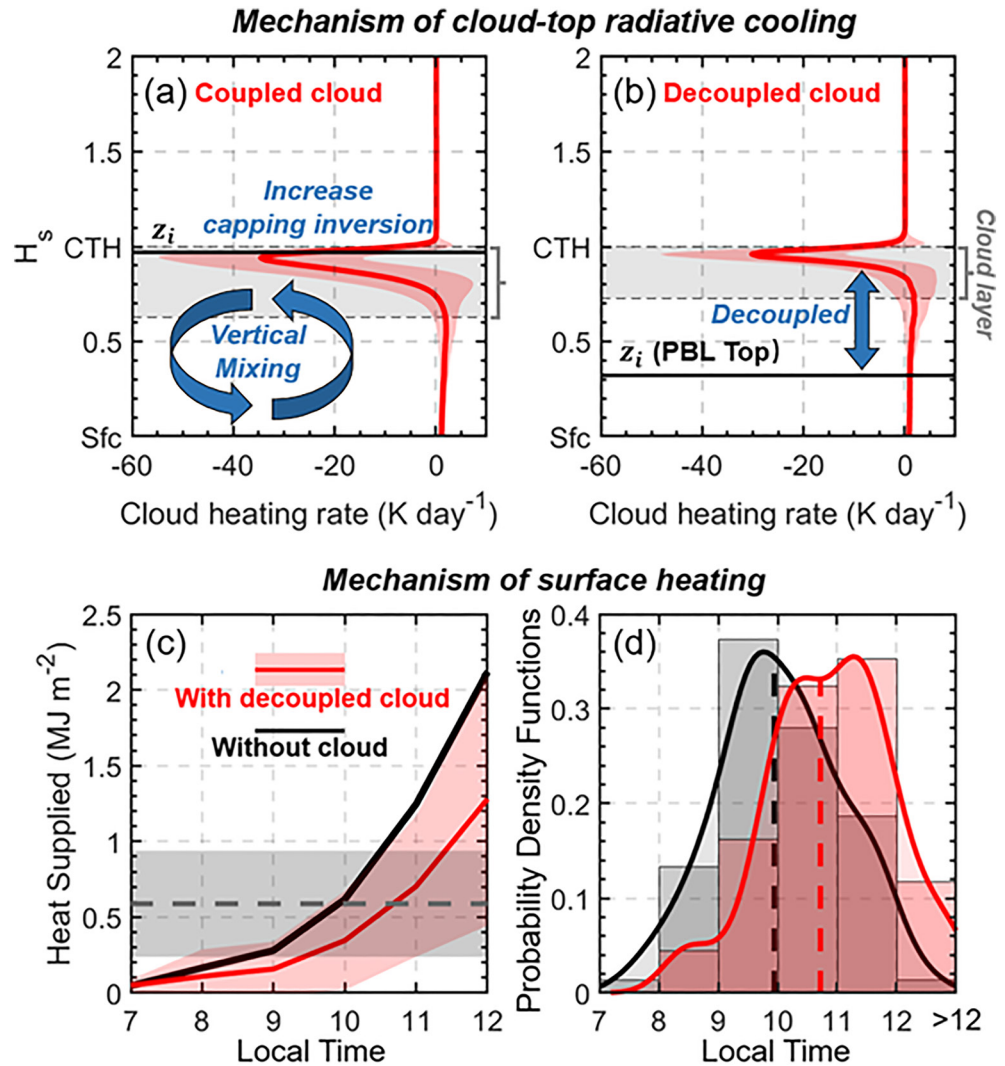
Figure 4. Mean profiles (red lines) and standard deviations (red shaded areas) of cloud heating rate for (a) coupled clouds and (b) decoupled clouds. The height coordinate (z) has been adjusted by CTH (cloud-top height) as $H_s = z/$CTH. The black lines and gray areas indicate the positions of PBL top (z_i) and cloud. (c) The red lines and shaded areas denote the mean and standard deviations of sensible heat supplied by surface for decoupled clouds, and the black line corresponds to heat supplied by surface without clouds. The gray line and shaded area indicate the mean and standard deviations of required heat for the phase transitions of PBL. (d) The probability density functions of the phase transitions with cloud radiative effects (red) and without cloud radiative effects (black), respectively.

condition maintains relatively shallow at a lower rate of growth until 10:00 LT, when the phase transition occurs. The delayed phase transition leads to ∼30% differences in the maximum PBL position.

Under the coupled conditions, the transition from stable to unstable PBL is not controlled by surface heating but by the CTRC. As noted in Figure 5c, an unstable PBL statistically occurs in the early morning (∼7:00 LT) under the coupled cloud conditions, much earlier than the phase transition for decoupled clouds and clear-sky conditions. Despite the early transition, CTRC also enhances the capping inversion and thus suppresses the growth of PBL (Figure 4a). As the net result, PBL exhibits a slow growth during the entire morning under the coupled cloud conditions, in contrast to the strong growth of PBL for other conditions after the phase transition.
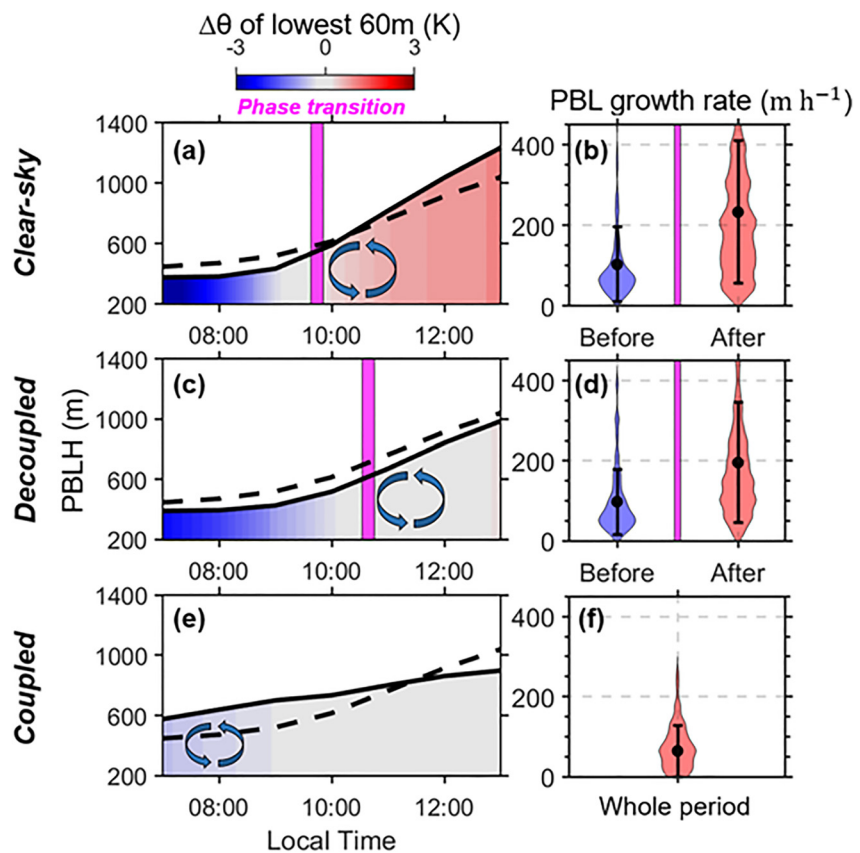
Figure 5. The temporal variations during 07:00-13:00 LT of the averaged PBLH variations for (a) clear sky, (c) decoupled clouds, and (e) coupled clouds. In (a, c, e), solid black lines indicate PBLH variations under different conditions, and dash black lines indicate the mean PBLH variations for all cases. The color shaded area indicates the $\Delta\theta = \theta_{surf} - \theta_{60m}$, which is indicator of stability within PBL (bounded by solid back lines). In (a, c), the mean phase transition times of PBL are marked as the pink area. In (b, d), the black dots and whiskers represent the means and standard deviation of PBL growth rates before and after the phase transition. For coupling conditions, there is no typical phase transition of PBL during the morning. In (f), the black dots and whiskers represent the average value and standard deviation of PBL growth rates during the whole period. The width of the color-shaded areas represents the corresponding distribution of PBL growth rates.

4. Conclusions

In this study, we use comprehensive ARM measurements over the SGP to investigate the impacts of cloud-surface coupling on the PBL morning transition from stable to unstable conditions. We also use the radiative transfer model and a deep-learning-based surface model to analyze the cloud radiative effects and the energy budget for the PBL phase transition. As the PBL turbulences drive the coupling between clouds and the surface, we consider coupling with the PBL to be equivalent to coupling with the land surface. The cloud-surface coupling has been discovered to alter the PBL phase transition mechanisms during the morning. Overall, decoupled clouds delay the PBL phase transition by significantly reducing the surface net radiation budget and sensible heat. Coupled clouds lead to the earlier transition from stable to unstable PBL triged by the CTRC.

The CTRC and surface heating are the two key processes associated with clouds to affect the PBL phase transitions. Under the coupled conditions, CTRC cools the air masses entrained from the free atmosphere. The cooled air sinks down through the PBL and facilitates the convections within the PBL. Quantitatively, both the radiative transfer model and radiosonde observations indicate that the CTRC can lead to a cooling rate of more than -1 K h^{-1} at the PBL top (Figures 3a and 4a), which can be regarded as the upside-down mechanism of surface heating. During the early morning, the CTRC is especially strong, leading to an unstable PBL without surface heating. Meanwhile, the CTRC can increase the capping inversion at the top of the cloud and PBL. The enhanced capping inversion effectively suppresses the growth of PBL because of the reverse relationship between the entrainment rate and capping inversion.

For decoupled clouds, CTRC cannot directly affect PBL development due to the decoupling between clouds and PBL. The surface heating mechanism plays a dominant role in driving the phase transition from stable to unstable PBL, and the same mechanism is valid under clear-sky conditions. As CRF decreases the energy supplied from surface fluxes, the PBL phase transition is delayed by 0.8-hr (standard deviation: 0.7-hr). Meanwhile, if the decreased energy from surface heating is smaller than the required energy for eroding the nocturnal inversion, the cloud radiative effect can prevent the occurrence of the phase transition process. This mechanism explains the previous observations of stable PBL during noontime (Zhang et al., 2018).

These changes in phase transitions induced by cloud-surface coupling led to large differences in PBL evolution. In particular, the delayed phase transition under the decoupled condition can lead to a notable reduction in the daily maximum PBLH compared to the clear sky. Meanwhile, the CTRC under the coupled condition leads to well-mixed PBLs with low growth rates during the morning. These findings attest to the important linkage between PBL development and cloud-surface coupling, which warrants explicit parameterizations in future studies.

Data Availability Statement

ARM radiosonde data are publicly available at the United States Department of Energy Atmospheric Radiation Measurement Data Center (https://www.arm.gov/capabilities/instruments/sonde). ARM Radiation measurements (QCRAD) are available at https://www.arm.gov/capabilities/vaps/qcrad. Surface sensible and latent heat fluxes are from the Bulk Aerodynamic Energy Balance Bowen Ratio data product (http://www.arm.gov/data/vaps/baebbr). (3) Cloud Optical Properties are obtained from the Multifilter Shadowband Radiometer (https://www.arm.gov/capabilities/vaps/mfrsrcldod). Cloud mask over SGP is publicly available at https://www.arm.gov/capabilities/vaps/arscl. The data of planetary boundary layer can be downloaded from https://doi.org/10.5281/zenodo.7374849.

References

Alemohammad, S. H., Fang, B., Konings, A. G., Aires, F., Green, J. K., Kolassa, J., et al. (2017). Water, energy, and carbon with artificial neural networks (WECANN): A statistically based estimate of global surface turbulent fluxes and gross primary productivity using solar-induced fluorescence. *Biogeosciences*, *14*(18), 4101–4124. https://doi.org/10.5194/bg-14-4101-2017

Bacmeister, J. T., Suarez, M. J., & Robertson, F. R. (2006). Rain reevaporation, boundary layer–convection interactions, and Pacific rainfall patterns in an AGCM. *Journal of the Atmospheric Sciences*, *63*(12), 3383–3403. https://doi.org/10.1175/jas3791.1

Bonan, G. B. (1996). *Land surface model (LSM version 1.0) for ecological, hydrological, and atmospheric studies: Technical description and users guide*. Technical note (No. PB-97-131494/XAB; NCAR/TN-417-STR). National Center for Atmospheric Research, Climate and Global Dynamics Div.

Brooks, I. M. (2003). I.M. Finding boundary layer top: Application of a wavelet covariance transform to lidar backscatter profiles. *Journal of Atmospheric and Oceanic Technology*, *20*(8), 1092–1105. https://doi.org/10.1175/1520-0426(2003)020<1092:fbltao>2.0.co;2

Burden, F., & Winkler, D. (2008). Bayesian regularization of neural networks. In *Artificial neural networks* (pp. 23–42).

Chu, Y., Li, J., Li, C., Tan, W., Su, T., & Li, J. (2019). Seasonal and diurnal variability of planetary boundary layer height in Beijing: Intercomparison between MPL and WRF results. *Atmospheric Research*, *227*, 1–13. https://doi.org/10.1016/j.atmosres.2019.04.017

Deardorff, J. W. (1976). On the entrainment rate of a stratocumulus-topped mixed layer. *Quarterly Journal of the Royal Meteorological Society*, *102*(433), 563–582. https://doi.org/10.1002/qj.49710243306

Dumedah, G., & Walker, J. P. (2014). Assessment of land surface model uncertainty: A crucial step towards the identification of model weaknesses. *Journal of Hydrology*, *519*, 1474–1484. https://doi.org/10.1016/j.jhydrol.2014.09.015

Garratt, J. R. (1994). The atmospheric boundary layer. *Earth-Science Reviews*, *37*(1–2), 89–134. https://doi.org/10.1016/0012-8252(94)90026-4

Garrett, A. J. (1982). A parameter study of interactions between convective clouds, the convective boundary layer, and a forested surface. *Monthly Weather Review*, *110*(8), 1041–1059. https://doi.org/10.1175/1520-0493(1982)110<1041:apsoib>2.0.co;2

Guo, J., Zhang, J., Yang, K., Liao, H., Zhang, S., Huang, K., et al. (2021). Investigation of near-global daytime boundary layer height using high-resolution radiosondes: First results and comparison with ERA5, MERRA-2, JRA-55, and NCEP-2 reanalyses. *Atmospheric Chemistry and Physics*, *21*(22), 17079–17097. https://doi.org/10.5194/acp-21-17079-2021

Hogan, R. J., Grant, A. L., Illingworth, A. J., Pearson, G. N., & O'Coannor, E. J. (2009). Vertical velocity variance and skewness in clear and cloud-topped boundary layers as revealed by Doppler lidar. *Quarterly Journal of the Royal Meteorological Society: A journal of the atmospheric sciences, applied meteorology and physical oceanography*, *135*(640), 635–643. https://doi.org/10.1002/qj.413

Jung, M., Reichstein, M., Margolis, H. A., Cescatti, A., Richardson, A. D., Arain, M. A., et al. (2011). Global patterns of land-atmosphere fluxes of carbon dioxide, latent heat, and sensible heat derived from eddy covariance, satellite, and meteorological observations. *Journal of Geophysical Research*, *116*(G3), G00J07. https://doi.org/10.1029/2010jg001566

Lock, A. P. (1998). The parametrization of entrainment in cloudy boundary layers. *Quarterly Journal of the Royal Meteorological Society*, *124*(552), 2729–2753. https://doi.org/10.1002/qj.49712455210

Nicholls, S. (1989). The structure of radiatively driven convection in stratocumulus. *Quarterly Journal of the Royal Meteorological Society*, *115*(487), 487–511. https://doi.org/10.1002/qj.49711548704

Prihodko, L., Denning, A. S., Hanan, N. P., Baker, I., & Davis, K. (2008). Sensitivity, uncertainty and time dependence of parameters in a complex land surface model. *Agricultural and Forest Meteorology*, *148*(2), 268–287. https://doi.org/10.1016/j.agrformet.2007.08.006

Ricchiazzi, P., Yang, S., Gautier, C., & Sowle, D. (1998). SBDART: A research and teaching software tool for plane-parallel radiative transfer in the Earth's atmosphere. *Bulletin of the American Meteorological Society*, *79*(10), 2101–2114. https://doi.org/10.1175/1520-0477(1998)079<2101:sarats>2.0.co;2

Rodriguez, J. D., Perez, A., & Lozano, J. A. (2009). Sensitivity analysis of k-fold cross validation in prediction error estimation. *IEEE Transactions on Pattern Analysis and Machine Intelligence*, *32*(3), 569–575. https://doi.org/10.1109/tpami.2009.187

Romps, D. M. (2017). Exact expression for the lifting condensation level. *Journal of the Atmospheric Sciences*, *74*(12), 3891–3900. https://doi.org/10.1175/jas-d-17-0102.1

Stull, R. B. (1988). *An introduction to boundary layer meteorology*. Springer Netherlands.

Su, T., Li, Z., & Kahn, R. (2020). A new method to retrieve the diurnal variability of planetary boundary layer height from lidar under different thermodynamic stability conditions. *Remote Sensing of Environment*, *237*, 111519. https://doi.org/10.1016/j.rse.2019.111519

Su, T., Li, Z., Zheng, Y., Wu, T., Wu, H., & Guo, J. (2022). Aerosol-boundary layer interaction modulated entrainment process. *NPJ Climate and Atmospheric Science*, *5*(1), 64. https://doi.org/10.1038/s41612-022-00283-1

Su, T., Zheng, Y., & Li, Z. (2022). Methodology to determine the coupling of continental clouds with surface and boundary layer height under cloudy conditions from lidar and meteorological data. *Atmospheric Chemistry and Physics*, *22*(2), 1453–1466. https://doi.org/10.5194/acp-22-1453-2022

Wallace, J. M., & Hobbs, P. V. (2006). *Atmospheric science: An introductory survey* (Vol. 92). Elsevier.

Wyngaard, J. C., & Coté, O. R. (1974). The evolution of a convective planetary boundary layer—A higher-order-closure model study. *Boundary-Layer Meteorology*, *7*(3), 289–308. https://doi.org/10.1007/bf00240833

Zhang, W., Guo, J., Miao, Y., Liu, H., Song, Y., Fang, Z., et al. (2018). On the summertime planetary boundary layer with different thermodynamic stability in China: A radiosonde perspective. *Journal of Climate*, *31*(4), 1451–1465. https://doi.org/10.1175/jcli-d-17-0231.1

Zheng, Y., Rosenfeld, D., & Li, Z. (2018). The relationships between cloud top radiative cooling rates, surface latent heat fluxes, and cloud-base heights in marine stratocumulus. *Journal of Geophysical Research: Atmospheres*, *123*(20), 11678–11690. https://doi.org/10.1029/2018jd028579

Zheng, Y., Zhang, H., Rosenfeld, D., Lee, S. S., Su, T., & Li, Z. (2021). Idealized large-eddy simulations of stratocumulus advecting over cold water. Part I: Boundary layer decoupling. *Journal of the Atmospheric Sciences*, *78*(12), 4089–4102.

References From the Supporting Information

Clothiaux, E. E., Ackerman, T. P., Mace, G. G., Moran, K. P., Marchand, R. T., Miller, M. A., & Martner, B. E. (2000). Objective determination of cloud heights and radar reflectivities using a combination of active remote sensors at the ARM CART sites. *Journal of Applied Meteorology*, *39*(5), 645–665. https://doi.org/10.1175/1520-0450(2000)039<0645:odocha>2.0.co;2

Flynn, D., Shi, Y., Lim, K., & Riihimaki, L. (2017). Cloud Type Classification (cldtype) value-added product. In R. Stafford (Ed.), *ARM research facility*. DOE/SC-ARM-TR-200.

Holdridge, D., Ritsche, M., Prell, J., & Coulter, R. (2011). Balloon-borne sounding system (SONDE) handbook. Retrieved from https://www.arm.gov/capabilities/instruments/sonde

Kollias, P., Clothiaux, E. E., Miller, M. A., Albrecht, B. A., Stephens, G. L., & Ackerman, T. P. (2007). Millimeter-wavelength radars: New Frontier in atmospheric cloud and precipitation research. *Bulletin of the American Meteorological Society*, *88*(10), 1608–1624. https://doi.org/10.1175/bams-88-10-1608

Liu, S., & Liang, X. Z. (2010). Observed diurnal cycle climatology of planetary boundary layer height. *Journal of Climate*, *23*(21), 5790–5809. https://doi.org/10.1175/2010jcli3552.1

Long, C. N., & Shi, Y. (2008). An automated quality assessment and control algorithm for surface radiation measurements. *The Open Atmospheric Science Journal*, *2*(1), 23–37. https://doi.org/10.2174/1874282300802010023

Tang, S., Xie, S., Zhang, M., Tang, Q., Zhang, Y., Klein, S. A., et al. (2019). Differences in eddy-correlation and energy-balance surface turbulent heat flux measurements and their impacts on the large-scale forcing fields at the ARM SGP site. *Journal of Geophysical Research: Atmospheres*, *124*(6), 3301–3318. https://doi.org/10.1029/2018jd029689

Wesely, M. L., Cook, D. R., & Coulter, R. L. (1995). *Surface heat flux data from energy balance Bowen ratio systems*. Argonne National Lab. (No. ANL/ER/CP-84065; CONF-9503104-2).